ARTICLES
PUBLISHED ONLINE: 7 NOVEMBER 2016 | DOI: 10.1038/NPHYS3947
nature physics

High-resolution studies of the Majorana atomic chain platform

Benjamin E. Feldman†, Mallika T. Randeria†, Jian Li†, Sangjun Jeon, Yonglong Xie, Zhijun Wang, Ilya K. Drozdov†‡, B. Andrei Bernevig and Ali Yazdani*

Ordered assemblies of magnetic atoms on the surface of conventional superconductors can be used to engineer topological superconducting phases and realize Majorana fermion quasiparticles (MQPs) in a condensed matter setting. Recent experiments have shown that chains of Fe atoms on Pb generically have the required electronic characteristics to form a one-dimensional topological superconductor and have revealed spatially resolved signatures of localized MQPs at the ends of such chains. Here we report higher-resolution measurements of the same atomic chain system performed using a dilution refrigerator scanning tunnelling microscope (STM). With significantly better energy resolution than previous studies, we show that the zero-bias peak (ZBP) in Fe chains has no detectable splitting from hybridization with other states. The measurements also reveal that the ZBP exhibits a distinctive 'double eye' spatial pattern on nanometre length scales. Theoretically we show that this is a general consequence of STM measurements of MQPs with substantial spectral weight in the superconducting substrate, a conclusion further supported by measurements of Pb overlayers deposited on top of the Fe chains. Finally, we report experiments performed with superconducting tips in search of the particle–hole symmetric MQP signature expected in such measurements.

Condensed matter systems provide a versatile platform for the realization of emergent phases that host exotic quasiparticles and exhibit novel electronic phenomena. Recently, there has been considerable interest in material systems in which superconductivity has a topological nature and Majorana fermion quasiparticle (MQP) excitations emerge either as edge modes or as core states of field-induced vortices[1–3]. The search for a solid state realization of MQPs has been motivated both by the possible discovery of a neutral fermion that is its own antiparticle, as first envisioned by Ettore Majorana[4], and by the prediction that solid state MQPs will obey non-Abelian statistics. The latter can be used to realize topological qubits for fault-tolerant quantum computation[5,6]. Initial searches for MQPs involved strongly interacting electron systems, such as fractional quantum Hall states[7–10]. However, more recent efforts have focused on engineering topological superconductivity by combining conventional superconductors and spin-textured electronic systems, such as the surface states of a topological insulator[11], Rashba semiconducting nanowires[12,13], or assemblies of magnetic atoms[14–24]. The key idea is that the spin texture of the electronic bands in these material platforms stabilizes an effective p-wave pairing through the proximity effect, and produces localized MQPs at the boundaries of the structure.

To date, strong evidence for the presence of MQPs has come from transport studies of hybrid superconductor–semiconductor nanowire devices[25], from scanning tunnelling microscope (STM) measurements of chains of magnetic atoms on the surface of a superconductor[23], and from STM measurements of vortices in superconductor–topological insulator heterostructures[26]. In proximitized semiconducting nanowires with strong spin–orbit interaction, transport studies showed a zero-bias peak (ZBP) for a range of parallel magnetic fields and gate voltages[25,27–29], as well as the fractional a.c. Josephson effect[30]. This is consistent with the appearance of a MQP when the field drives these nanowires into the topological phase. More recent experiments demonstrated the expected change in charging that is characteristic of such a nanowire in the topological phase, as well as experimental signatures of exponentially suppressed coupling between MQP end modes[31]. A recent effort aims to discount alternative explanations for the ZBP, such as the Kondo effect or disorder[32–36], by examining cleaner nanowire devices[37].

Chains of magnetic atoms on the surface of a superconductor provide a novel approach to engineer topological superconductivity, with the unique advantage that MQPs can be directly visualized using spatially resolved STM measurements. Previous spin-polarized STM studies of self-assembled chains of Fe atoms on superconducting Pb showed clear evidence for both ferromagnetic ordering of the Fe atoms and strong spin–orbit coupling at the surface of the Pb substrate[23]. The combination of these two ingredients together with proximity-induced superconductivity is predicted to almost always produce a topological superconducting phase in such atomic chains[24]. Consistent with this prediction, spatially resolved spectroscopic measurements showed the presence of a ZBP in the local density of states (LDOS) at the end of the chains, as expected for a localized MQP[23]. Subsequent experiments have probed the properties of Fe chains on Pb with superconducting tips and have reported similar zero-energy states, as well as explored other features on this platform[38,39].

The ZBP in these chains was shown not to be due to the Kondo effect, as it is fully suppressed when a small magnetic field (well below the Kondo temperature) is applied to drive the Pb substrate normal. However, other questions regarding the MQP interpretation of the ZBP for atomic chains require more detailed

Joseph Henry Laboratories and Department of Physics, Princeton University, Princeton, New Jersey 08544, USA. †These authors contributed equally to this work. ‡Present address: Condensed Matter Physics and Materials Science Department, Brookhaven National Laboratory, Upton, New York 11973, USA. *e-mail: yazdani@princeton.edu

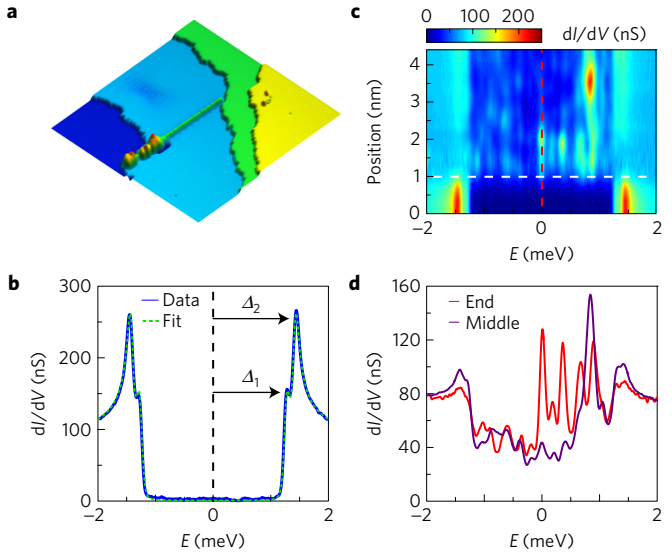

Figure 1 | Zero-bias end mode in Fe chains on Pb. a, Three-dimensional rendering of an Fe chain on the Pb(110) surface. Scan area is 50 nm × 50 nm, and the z height range is 7.8 Å. Setpoint bias $V_{set} = -50$ mV and current $I_{set} = 200$ pA. **b**, Differential conductance dI/dV of the bare Pb(110) surface (blue) and its two-gap fit (green) with $\Delta_1 = 1.26$ meV and $\Delta_2 = 1.42$ meV, at fixed temperature $T = 250$ mK using a broadening $\Gamma = 8$ μeV. **c**, Linecut of dI/dV along the side of an Fe chain, showing a sharp zero-bias peak (ZBP) localized to the end, as well as several subgap Shiba states. The white dashed line marks the end of the Fe chain. **d**, dI/dV at the chain end (red) and its average in the middle of the chain (purple; averaged over positions >2.5 nm).

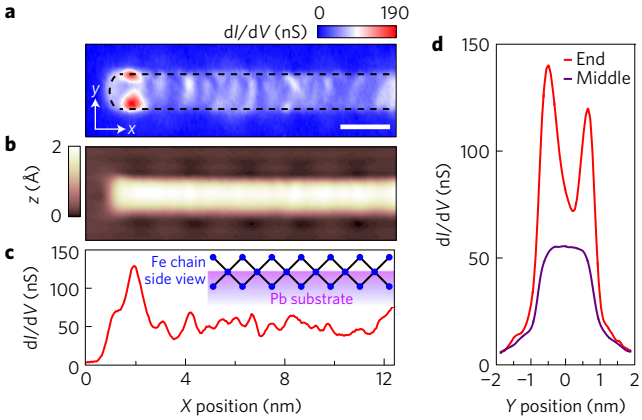

Figure 2 | 'Double eye' pattern and spatial dependence of the ZBP. **a**,**b**, Map of the zero-bias conductance (**a**) along a chain and its corresponding topography (**b**). Scale bar, 2 nm. **c**,**d**, dI/dV as a function of position along (**c**) and transverse to (**d**) the Fe chain. Data in **c** are averaged over the 1.6 nm chain width. Inset: schematic of a zigzag Fe chain partially embedded in the substrate. In **d**, the end spectrum (red) is averaged over the 1 nm length of the 'double eye' feature, and the mid-chain spectrum (purple) is averaged over the remainder of the chain.

investigation. Initially, the nanometre length scale reported for the localization of MQPs from spectroscopic mapping was suggested to be inconsistent with the small predicted p-wave gap[40]. Subsequent theoretical efforts from several groups, however, have shown that the short MQP localization length is expected due to strong velocity renormalization in this hybrid system; the characteristic MQP localization length is much shorter than the coherence length of the host superconductor[24,41]. Another concern is the temperature at which the previous measurements were performed (around 1 K), which is comparable to the expected size of the p-wave gap. The temperature limited the precision with which previous experiments could determine the possible splitting of the ZBP. A very accurate energy resolution could distinguish a MQP from a pair of states very close to zero energy, and could also enable detailed examination of the background of low-energy electronic states.

The focus of the current study is to extend the previous experiments to a lower temperature that allows us to probe the magnetic atomic chains with much higher energy resolution. We demonstrate that the ZBP in atomic Fe chains remains pinned at zero energy with no detectable hybridization with other electronic states, and we reveal new information about the background of low-energy quasiparticle (Shiba[42–44]) states. We also provide the first experimental evidence that the ZBP has substantial weight in the host superconductor, based on the observation of a characteristic 'double eye' spatial pattern of the zero-bias conductance, as well as measurements of Fe chains that have been covered with a monolayer of Pb. We develop theoretical models that accurately describe both the detailed nature of the states within the Fe chains, as well as the observation of enhanced MQP weight in the superconducting substrate. Finally, we describe experiments using superconducting tips at lower temperatures motivated by a recent proposal for detecting the particle–hole symmetry of MQPs[39,45]. Taken together, these results provide significant evidence in support of the MQP interpretation of the ZBP in the Fe/Pb atomic chain system.

High-resolution spectroscopic mapping of the zero mode

We extend the previous experiments to lower temperature using a dilution refrigerator STM[46], which cools samples to about 20 mK. We fabricate atomically ordered one-dimensional Fe chains on a pristine Pb(110) surface as described in ref. 23, yielding chains up to 40 nm in length with pristine portions ranging from 5 to 20 nm (Fig. 1a). Measurements of the LDOS with normal tips far from the chains reveal spectral features associated with the two energy gaps expected from the two Fermi surfaces of Pb[47], and the data fit well to theory using an electron temperature of 250 mK (Fig. 1b). The majority of the Fe chains that we have explored show a prominent ZBP in spectroscopic measurements near their end (Fig. 1c) and exhibit no sign that it is offset from zero bias or split by hybridization with other states, with an experimental upper bound of 80 μeV splitting. As shown in Fig. 1d, the full-width at half-maximum of the ZBP can be as low as 90 μeV (above the background measured in the middle of the chain), which is comparable to the thermal broadening expected at 250 mK. In contrast, no prominent ZBP is apparent in the bulk of the chain (Fig. 1d), where the spectra typically show a set of about 9–10 resonances within the energy window of the host Pb gap. These resonances are asymmetric in spectral weight, but appear to be close to symmetric in energy about zero, suggesting that they are energetically resolved (see Supplementary Methods). The first peak in the spectra above zero bias is typically about ±150–250 μeV—a value consistent with previous measurements using superconducting tips at higher temperatures[23].

In contrast to measurements at 1.4 K, the ZBP at the end of the chain in the millikelvin temperature experiments can reach more than 1.6 times the normal state conductance above the superconducting Pb gap (see Fig. 1d for example). The ZBP scales approximately proportionally with the conductance set by the tunnel junction impedance, reaching a maximum value of about $0.16e^2/h$, obtained with a 250 kΩ junction impedance (see Supplementary Methods). This value is still smaller than the predicted universal conductance of $2e^2/h$ for a MQP[48], suggesting that we are in the sequential tunnelling regime and the temperature of our measurements is still large compared to the tunnelling energy scale for coupling between the MQP and the STM tip. Nonetheless,

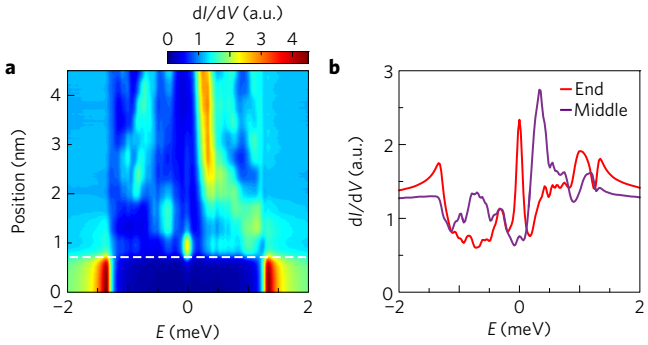

Figure 3 | Theoretical model of the zero-bias end mode. a, Simulation of d*I*/d*V* as a function of position along the chain, whose end is marked by the white dashed line. **b**, Theoretically predicted d*I*/d*V* at the end (red) and in the middle (purple) of the Fe chain. A ZBP localized to the end of the chain and subgap Shiba states that qualitatively resemble the experimental data are apparent.

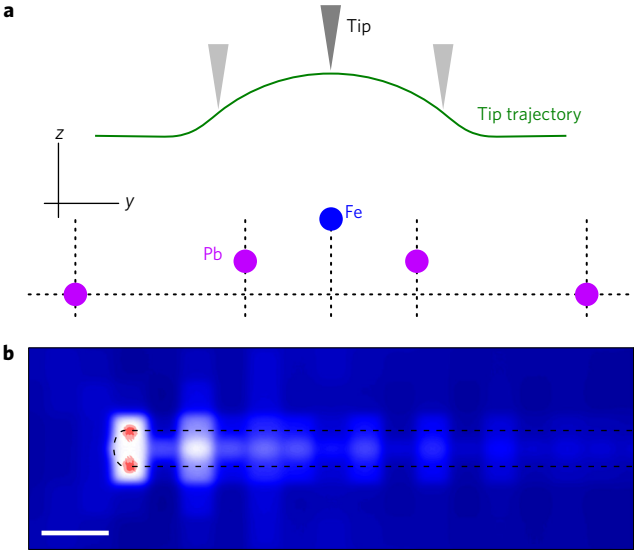

Figure 4 | Theoretical model of the 'double eye' spatial pattern of the ZBP. **a**, Schematic illustration of the topmost Fe atom of the chain and underlying substrate topography, as determined from DFT calculations, and the tip trajectory during measurements. **b**, Simulation of the expected zero-bias conductance as a function of position. A 'double eye' pattern of the ZBP is apparent, consistent with the experimental observations. The dashed black line corresponds to the theoretically predicted topographic signal within this model. Scale bar, two Pb lattice constants.

the absence of hybridization with other states, judged by the almost thermally limited width of the ZBP, and our observation that the spectral weight of the zero mode is enhanced (relative to the background) at lower temperatures are significant steps in supporting the MQP interpretation of the ZBP in Fe chains. We also note that the ZBP is isolated in energy and position from other Shiba states, so it is not caused by a trivial Shiba state whose energy disperses as the chain diameter tapers near its end[49].

Having established the presence of a sharp ZBP, we examine its spatial structure by comparing zero-bias conductance maps and topographic measurements on the same chain, as shown in Fig. 2a,b. The conductance map confirms that the ZBP is localized at the chain ends, and also reveals an intriguing spatial pattern. The maximum of the ZBP is not centred on the Fe chain, but instead exhibits twin peaks situated near its sides. This characteristic 'double eye' feature was observed in many different chains (approximately two-thirds of those explored); additional examples are presented in the Supplementary Methods. The 'double eye' conductance pattern underscores the importance of tip positioning to detect the strongest ZBP, and may help explain some of the variability in results reported by other groups[39]. Along the chain, the zero-bias conductance typically decays within one nanometre to a characteristic value around 40–50% of the normal state conductance in the middle of the chain, with small oscillations in amplitude (Fig. 2c). This residual zero-bias conductance probably results from a combination of thermally broadened Shiba states and the exponentially decaying tail of the zero-energy end state (see Supplementary Methods). A cross-section of zero-bias conductance transverse to the wire axis at its end, presented in Fig. 2d, also shows the rapid decay of the zero-bias state from the Fe into the Pb substrate. Despite this rapid decay, we show below that the 'double eye' feature results from substantial MQP spectral weight in the Pb atoms adjacent to the Fe chain.

Modelling the spectroscopic properties of Fe chains

To understand the spectroscopic features of the Fe chains and their spatial dependence, we perform model calculations that take into account the chain structure, the hybridization of its electronic states with the Pb substrate, and the influence of the STM tip trajectory on the measurements. Previous studies[23] determined that the most likely structure for the atomic Fe chains is a single atom wide, with three atoms stacked vertically in a zigzag structure that is partially embedded between the rows of the Pb(110) surface (Fig. 2c, inset). Following the numerical approach outlined in ref. 24, we compute the spectroscopic properties of the embedded zigzag Fe chain and compare them with the results of our STM measurements (see Supplementary Methods for model parameters).

Figure 3 shows the calculated LDOS as a function of energy and position along a chain of finite length (21 nm), which can be compared with the data in Fig. 1. The model calculations qualitatively match the experimental results: they show a pronounced ZBP that is localized to the end of the Fe chain, as well as substantial subgap spectral weight throughout the chain whose amplitude is electron–hole asymmetric. The observed experimental variation of the spectra along the chain probably results in part from modulation of the Fe atomic chain structure due to incommensurability with the Pb substrate (not included in the model), as well as finite size effects. Nevertheless, the extended profiles of the subgap states along the chain, seen in both experiments and model calculations, strongly suggest that these subgap states are manifestations of thermally broadened van Hove singularities of Shiba bands induced by the Fe chain into the Pb gap. The model calculations also show that although the thermal broadening does not preclude us from observing the ZBP due to the MQP, it does prevent the observation of a hard *p*-wave gap. This is similar to recently published data on semiconductor nanowires[31], where the hard gap obtained at zero field becomes softer than the one presented here in the presence of a magnetic field—the regime in which the ZBP is observed. Finally, our model reproduces the experimentally observed rapid decay of the ZBP associated with the MQP at the end of the chain.

To understand the origin of the 'double eye' spatial structure of the ZBP, we use a simple three-site model that takes into account the MQP spectral weight on the Fe and Pb sites, as well as the influence of the trajectory of the STM tip on the conductance (Fig. 4a). This model, whose details are included in the Supplementary Methods, shows that the conductance at zero energy will have a double-peak structure transverse to the chain when the ratio of the LDOS at zero energy for the Fe site [$\rho_{Fe}(0)$] relative to the Pb sites [$\rho_{Pb}(0)$] is less than the ratio of the integral of the LDOS at these sites (ρ_{Fe}, ρ_{Pb}) over the energy window set by the voltage bias. Such a condition

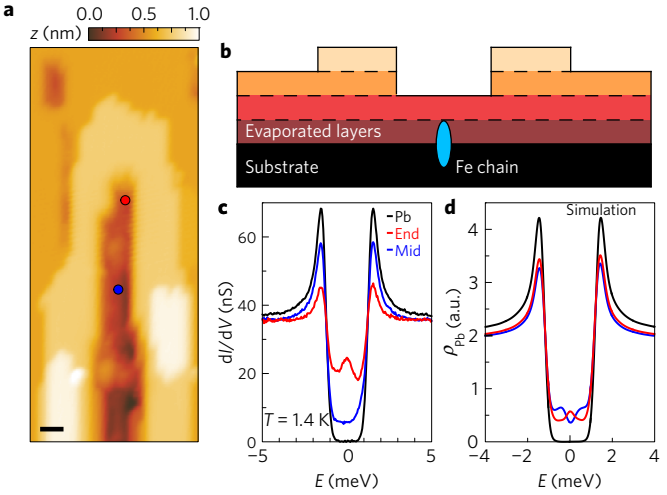

Figure 5 | ZBP in Pb overlayer above Fe chain. a, Topography of a buried Fe chain. $V_{set} = 90$ mV and $I_{set} = 100$ pA. Scale bar, 2 nm. **b**, Corresponding schematic showing the chain covered with a single monolayer of Pb. **c**, dI/dV at the end of the chain (red), in the middle (blue) and on the bare Pb substrate (black). $V_{set} = 5$ mV and $I_{set} = 700$ pA. **d**, Theoretically calculated LDOS of the Pb atoms neighbouring the Fe chain at its end (red) and middle (blue), and on the bare Pb substrate (black).

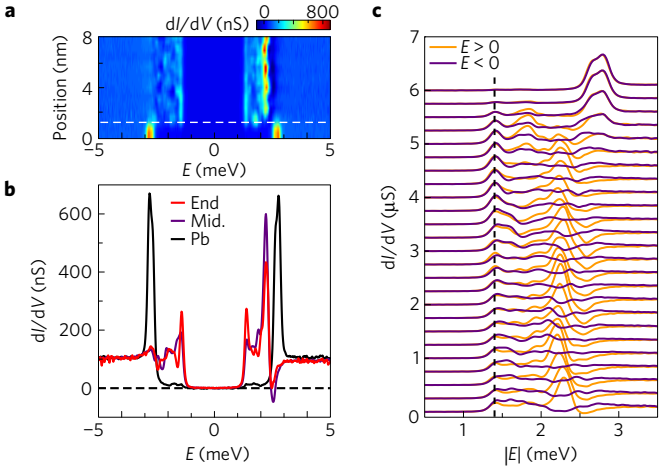

Figure 6 | Superconducting tip spectra and electron–hole symmetry of the zero-energy end mode. a, dI/dV along the side of an Fe chain, showing an end mode at $e|V| = \Delta_{tip}$. The white dashed line marks the end of the chain. **b**, Individual dI/dV spectra on the bare Pb (black) and at the end (red) and middle (purple) of the Fe chain. The end spectrum shows electron–hole symmetric peak amplitude at $e|V| = \Delta_{tip}$. **c**, dI/dV spectra at each position in **a**, plotted as a function of $|E|$, with each curve offset for clarity (top spectrum corresponds to 0 nm in **a**). The end mode at $e|V| = \Delta_{tip}$ is electron–hole symmetric in amplitude, whereas states at higher energies are not. A weaker peak at $e|V| = \Delta_{tip}$ is also visible in the middle of the chain; its origin is probably the same as the residual spectral weight at zero bias measured in the middle of the Fe chains using normal tips.

can be satisfied because of several realistic factors. First, because the number of orbitals on the Fe atoms in the normal state is larger than that on the Pb atoms, we generically expect $\rho_{Fe}/\rho_{Pb} > 1$. Second, and more important, the strong suppression of the local order parameter on the Pb atoms near the Fe chain[50], as well as the adapted structure caused by strong bonding between the Fe chain and its nearby Pb atoms[23], results in a significant enhancement of the subgap LDOS [including $\rho_{Pb}(0)$] in the superconducting substrate adjacent to the chain. Consequently, we find that $\rho_{Fe}/\rho_{Pb} > \rho_{Fe}(0)/\rho_{Pb}(0)$ (see Supplementary Methods), and we therefore expect tunnelling into the MQP to be larger on the sides of the chain as opposed to its centre. The results of our simulations including these realistic factors are shown in Fig. 4b, and they demonstrate a clear double-peak structure similar to the experimental observations. The model described above therefore shows that the 'double eye' spatial pattern observed in experiment results from substantial MQP weight in the host superconductor.

Buried Fe chains and MQP signature in Pb overlayers

We further investigate the idea that the MQP can have significant spectral weight in the host superconductor by examining Fe chains covered with a monolayer of Pb (Fig. 5a,b). Encapsulating Fe chains with Pb may also influence the strength of the proximity-induced superconductivity; similar experiments on semiconducting nanowires have very recently been explored[31,51]. We perform spectroscopic measurements on the buried Fe chains at 1.4 K (Fig. 5c), which show a ZBP localized close to what we determine to be the end of such chains, based on a comparison of spectroscopic and topographic maps. The background in-gap conductance measured on the Pb overlayers is typically much lower than that measured on top of exposed chains, and it is also nearly electron–hole symmetric. This electron–hole symmetry is also seen in our model calculations when we examine the spectral properties on the Pb sites below the Fe chain (Fig. 5d), and it is probably a consequence of the basic symmetry of the states in the host superconductor. The suppression of the low-energy states except the zero mode in these Pb overlayers suggests that the pairing strength of the Fe chain may be enhanced in this geometry. This possibility, together with the observation of a robust ZBP (although broad in this case because of measurement at 1.4 K), indicates that the buried chain geometry may have some key advantages for future studies of MQPs; especially with regard to braiding. Manipulating MQPs in buried circular chain geometries might provide a clean signal without interference from other Shiba states[52].

Probing the MQP electron–hole symmetry

As a final test of the MQP interpretation of our experiment, we perform measurements with superconducting tips to investigate the electron–hole symmetry of the zero-energy state. Previous studies[23,39] of the Fe/Pb atomic chain system have used superconducting tips to achieve higher spectroscopic resolution and to explore the MQP particle–hole symmetry at temperatures of about 1 K. The measurements showed asymmetric (in amplitude) peaks at a voltage corresponding to the superconducting gap of the tip ($eV = \pm\Delta_{tip}$), as well as other in-gap states at higher energies, and they were interpreted to suggest that some of the spectral weight of the zero-energy mode may result from trivial states[39].

We have extended these measurements to lower temperatures in our dilution refrigerator STM, as shown in Fig. 6. Here we show a linecut of spectra along the wire, positioned so that we cross one of the eyes of the ZBP. Whereas previous work at about 1 K found that spectroscopic measurements with superconducting tips show considerably better energy resolution than normal tips, we do not find that this improvement continues at lower temperatures. Instead, the width of the ZBP and other in-gap states resolved with the superconducting tips are slightly broader (120 μeV, at best) than measurements of the same electronic features with the normal tips (90 μeV, at best). This difference may result from an imperfect tip containing quasiparticle excitations, perhaps due to the amorphous nature or small size of the superconducting apex.

Regardless, spectroscopy with a superconducting tip has been proposed as a way to demonstrate the particle–hole symmetry of the MQP, which should produce peaks with symmetric amplitude at $eV = \pm\Delta_{tip}$, as opposed to trivial Shiba states near zero energy,

which could have asymmetric amplitude[39,45]. As shown in Fig. 6 for one particular tip and Fe chain, we indeed observe two symmetric peaks at $eV = \pm\Delta_{tip} \sim 1.35$ meV, a behaviour that is distinct from the electron–hole asymmetry of all other in-gap features, especially that associated with a Shiba band at $eV \sim 2$ meV. While we have found a few combinations of chains and superconducting tips that show symmetric peaks at $eV = \pm\Delta_{tip}$ at the end of the chain, we sometimes also observe non-symmetric behaviour (see Supplementary Methods). Further efforts are required to determine the experimental conditions that lead to the symmetric peaks expected for MQPs, and whether the condition of the tip and sample can influence such measurements.

Concluding remarks and outlook

Performing high-resolution measurements of our atomic chain platform at lower temperatures allows us to place a stringent upper bound of 80 μeV splitting of the ZBP. In addition, the 'double eye' spatial pattern of the ZBP and its robustness to the deposition of a superconducting overlayer demonstrate the enhanced MQP spectral weight in the host superconductor. The detailed correspondence between these data and theoretical modelling provides critical experimental evidence for the predicted topological nature of superconductivity in this system and the interpretation of the edge bounded ZBPs as signatures of localized MQPs. Further investigations of this platform would, however, advance more rapidly if the structure and magnetic properties of the chains could be manipulated and optimized. For example, the complex in-gap structure of our chains is a consequence of their zigzag structure, which gives rise to multiple Shiba bands[24]. Future efforts in constructing such chains using a STM to perform atomic manipulation may be used to build simpler chains, as well as provide the opportunity to maximize the induced superconducting pairing within them. The magnetism in such chains also plays a critical role in the emergent topological superconductivity, and it needs to be studied to determine the phase diagram of superconducting phases in such chains[24,41]. Finally, using thin-film superconducting substrates would provide an opportunity to use a parallel magnetic field as a tuning parameter of the properties of chains or other assemblies of magnetic adatoms on their surface, and perhaps ultimately to manipulate MQPs in this platform[52].

Methods

Methods, including statements of data availability and any associated accession codes and references, are available in the online version of this paper.

Received 19 June 2016; accepted 4 October 2016; published online 7 November 2016

References

1. Kitaev, A. Y. Unpaired Majorana fermions in quantum wires. *Phys.-Usp.* **44,** 131–136 (2001).
2. Alicea, J. New directions in the pursuit of Majorana fermions in solid state systems. *Rep. Progr. Phys.* **75,** 076501 (2012).
3. Beenakker, C. W. J. Search for Majorana fermions in superconductors. *Ann. Rev. Condens. Matter Phys.* **4,** 113–136 (2013).
4. Majorana, E. Teoria simmetrica dell'elettrone e del positrone. *Il Nuovo Cimento* **14,** 171–184 (1937).
5. Kitaev, A. Y. Fault-tolerant quantum computation by anyons. *Ann. Phys.* **303,** 2–30 (2003).
6. Nayak, C., Simon, S. H., Stern, A., Freedman, M. & Das Sarma, S. Non-Abelian anyons and topological quantum computation. *Rev. Mod. Phys.* **80,** 1083–1159 (2008).
7. Salomaa, M. M. & Volovik, G. E. Cosmiclike domain walls in superfluid ^{3}He-*B*: instantons and diabolical points in (k,r) space. *Phys. Rev. B* **37,** 9298–9311 (1988).
8. Ivanov, D. A. Non-abelian statistics of half-quantum vortices in *p*-wave superconductors. *Phys. Rev. Lett.* **86,** 268–271 (2001).
9. Moore, G. & Read, N. Nonabelions in the fractional quantum Hall-effect. *Nuclear Phys. B* **360,** 362–396 (1991).
10. Read, N. & Green, D. Paired states of fermions in two dimensions with breaking of parity and time-reversal symmetries and the fractional quantum Hall effect. *Phys. Rev. B* **61,** 10267–10297 (2000).
11. Fu, L. & Kane, C. L. Superconducting proximity effect and Majorana fermions at the surface of a topological insulator. *Phys. Rev. Lett.* **100,** 096407 (2008).
12. Lutchyn, R. M., Sau, J. D. & Das Sarma, S. Majorana fermions and a topological phase transition in semiconductor–superconductor heterostructures. *Phys. Rev. Lett.* **105,** 077001 (2010).
13. Oreg, Y., Refael, G. & von Oppen, F. Helical liquids and Majorana bound states in quantum wires. *Phys. Rev. Lett.* **105,** 177002 (2010).
14. Choy, T. P., Edge, J. M., Akhmerov, A. R. & Beenakker, C. W. J. Majorana fermions emerging from magnetic nanoparticles on a superconductor without spin–orbit coupling. *Phys. Rev. B* **84,** 195442 (2011).
15. Kjaergaard, M., Wölms, K. & Flensberg, K. Majorana fermions in superconducting nanowires without spin–orbit coupling. *Phys. Rev. B* **85,** 020503 (2012).
16. Nadj-Perge, S., Drozdov, I. K., Bernevig, B. A. & Yazdani, A. Proposal for realizing Majorana fermions in chains of magnetic atoms on a superconductor. *Phys. Rev. B* **88,** 020407 (2013).
17. Pientka, F., Glazman, L. I. & von Oppen, F. Topological superconducting phase in helical Shiba chains. *Phys. Rev. B* **88,** 155420 (2013).
18. Klinovaja, J., Stano, P., Yazdani, A. & Loss, D. Topological superconductivity and Majorana fermions in RKKY systems. *Phys. Rev. Lett.* **111,** 186805 (2013).
19. Braunecker, B. & Simon, P. Interplay between classical magnetic moments and superconductivity in quantum one-dimensional conductors: toward a self-sustained topological Majorana phase. *Phys. Rev. Lett.* **111,** 147202 (2013).
20. Vazifeh, M. M. & Franz, M. Self-organized topological state with Majorana fermions. *Phys. Rev. Lett.* **111,** 206802 (2013).
21. Nakosai, S., Tanaka, Y. & Nagaosa, N. Two-dimensional *p*-wave superconducting states with magnetic moments on a conventional *s*-wave superconductor. *Phys. Rev. B* **88,** 180503 (2013).
22. Rontynen, J. & Ojanen, T. Topological superconductivity and high Chern numbers in 2D ferromagnetic Shiba lattices. *Phys. Rev. Lett.* **114,** 236803 (2015).
23. Nadj-Perge, S. *et al*. Observation of Majorana fermions in ferromagnetic atomic chains on a superconductor. *Science* **346,** 602–607 (2014).
24. Li, J. *et al*. Topological superconductivity induced by ferromagnetic metal chains. *Phys. Rev. B* **90,** 235433 (2014).
25. Mourik, V. *et al*. Signatures of Majorana fermions in hybrid superconductor–semiconductor nanowire devices. *Science* **336,** 1003–1007 (2012).
26. Sun, H.-H. *et al*. Majorana zero mode detected with spin selective Andreev reflection in the vortex of a topological superconductor. *Phys. Rev. Lett.* **116,** 257003 (2016).
27. Das, A. *et al*. Zero-bias peaks and splitting in an Al–InAs nanowire topological superconductor as a signature of Majorana fermions. *Nat. Phys.* **8,** 887–895 (2012).
28. Deng, M. T. *et al*. Anomalous zero-bias conductance peak in a Nb–InSb nanowire–Nb hybrid device. *Nano Lett.* **12,** 6414–6419 (2012).
29. Finck, A. D. K., Van Harlingen, D. J., Mohseni, P. K., Jung, K. & Li, X. Anomalous modulation of a zero-bias peak in a hybrid nanowire-superconductor device. *Phys. Rev. Lett.* **110,** 126406 (2013).
30. Rokhinson, L. P., Liu, X. & Furdyna, J. K. The fractional a.c. Josephson effect in a semiconductor–superconductor nanowire as a signature of Majorana particles. *Nat. Phys.* **8,** 795–799 (2012).
31. Albrecht, S. M. *et al*. Exponential protection of zero modes in Majorana islands. *Nature* **531,** 206–209 (2016).
32. Liu, J., Potter, A. C., Law, K. T. & Lee, P. A. Zero-Bias peaks in the tunneling conductance of spin-orbit-coupled superconducting wires with and without Majorana end-states. *Phys. Rev. Lett.* **109,** 267002 (2012).
33. Lee, E. J. H. *et al*. Zero-bias anomaly in a nanowire quantum dot coupled to superconductors. *Phys. Rev. Lett.* **109,** 186802 (2012).
34. Churchill, H. O. H. *et al*. Superconductor-nanowire devices from tunneling to the multichannel regime: zero-bias oscillations and magnetoconductance crossover. *Phys. Rev. B* **87,** 241401 (2013).
35. Pikulin, D. I., Dahlhaus, J. P., Wimmer, M., Schomerus, H. & Beenakker, C. W. J. A zero-voltage conductance peak from weak antilocalization in a Majorana nanowire. *New J. Phys.* **14,** 125011 (2012).
36. Kells, G., Meidan, D. & Brouwer, P. W. Near-zero-energy end states in topologically trivial spin–orbit coupled superconducting nanowires with a smooth confinement. *Phys. Rev. B* **86,** 100503 (2012).
37. Zhang, H. *et al*. Ballistic Majorana nanowire devices. Preprint at http://arXiv.org/abs/1603.04069 (2016).

38. Pawlak, R. *et al*. Probing atomic structure and Majorana wavefunctions in mono-atomic Fe-chains on superconducting Pb-surface. Preprint at http://arXiv.org/abs/1505.06078 (2015).
39. Ruby, M. *et al*. End states and subgap structure in proximity-coupled chains of magnetic adatoms. *Phys. Rev. Lett.* **115,** 197204 (2015).
40. Dumitrescu, E., Roberts, B., Tewari, S., Sau, J. D. & DasSarma, S. Majorana fermions in chiral topological ferromagnetic nanowires. *Phys. Rev. B* **91,** 094505 (2015).
41. Peng, Y., Pientka, F., Glazman, L. I. & von Oppen, F. Strong localization of Majorana end states in chains of magnetic adatoms. *Phys. Rev. Lett.* **114,** 106801 (2015).
42. Yu, L. Bound state in superconductors with paramagnetic impurities. *Acta Phys. Sin.* **21,** 75–91 (1965).
43. Shiba, H. Classical spins in superconductors. *Progr. Theor. Phys.* **40,** 435–451 (1968).
44. Rusinov, A. I. On theory of gapless superconductivity in alloys containing paramagnetic impurities. *Sov. Phys. Jetp-Ussr* **29,** 1101–1106 (1969).
45. Peng, Y., Pientka, F., Vinkler-Aviv, Y., Glazman, L. I. & von Oppen, F. Robust Majorana conductance peaks for a superconducting lead. *Phys. Rev. Lett.* **115,** 266804 (2015).
46. Misra, S. *et al*. Design and performance of an ultra-high vacuum scanning tunneling microscope operating at dilution refrigerator temperatures and high magnetic fields. *Rev. Sci. Instrum.* **84,** 103903 (2013).
47. Ruby, M., Heinrich, B. W., Pascual, J. I. & Franke, K. J. Experimental demonstration of a two-band superconducting state for lead using scanning tunneling spectroscopy. *Phys. Rev. Lett.* **114,** 157001 (2015).
48. Law, K. T., Lee, P. A. & Ng, T. K. Majorana fermion induced resonant Andreev reflection. *Phys. Rev. Lett.* **103,** 237001 (2009).
49. Sau, J. D. & Brydon, P. M. R. Bound states of a ferromagnetic wire in a superconductor. *Phys. Rev. Lett.* **115,** 127003 (2015).
50. Meng, T., Klinovaja, J., Hoffman, S., Simon, P. & Loss, D. Superconducting gap renormalization around two magnetic impurities: from Shiba to Andreev bound states. *Phys. Rev. B* **92,** 064503 (2015).
51. Krogstrup, P. *et al*. Epitaxy of semiconductor–superconductor nanowires. *Nat. Mater.* **14,** 400–406 (2015).
52. Li, J., Neupert, T., Bernevig, B. A. & Yazdani, A. Manipulating Majorana zero modes on atomic rings with an external magnetic field. *Nat. Commun.* **7,** 10395 (2016).

Acknowledgements

The work at Princeton has been supported by ONR-N00014-14-1-0330, ONR-N00014-11-1-0635, ONR-N00014-13-10661, NSF-MRSEC programs through the Princeton Center for Complex Materials DMR-142054, NSF-DMR-1104612, NSF-DMR-1420541, NSF EAGER Award NOA-AWD1004957, DOE DE-SC0016239, Simons Investigator Award, Packard Foundation and Schmidt Fund for Innovative Research, and by the Gordon and Betty Moore Foundation as part of EPiQS initiative (GBMF4530). This project was also made possible using the facilities at Princeton Nanoscale Microscopy Laboratory supported by grants through ARO-MURI Program W911NF-12-1-0461, DOE-BES, LPS and ARO-W911NF-1-0606, and Eric and Wendy Schmidt Transformative Technology Fund at Princeton. B.E.F. acknowledges financial support from the Dicke Fellowship. M.T.R. acknowledges support from the NSF Graduate Research Fellowship Program.

Author contributions

B.E.F., M.T.R. and I.K.D. performed the dilution refrigerator STM measurements. S.J., Y.X. and I.K.D. conducted the measurements on Fe chains capped with Pb overlayers. J.L., Z.W. and B.A.B. performed the theoretical modelling and simulations. All authors contributed to analysing the data and writing the manuscript.

Additional information

Supplementary information is available in the online version of the paper. Reprints and permissions information is available online at www.nature.com/reprints. Correspondence and requests for materials should be addressed to A.Y.

Competing financial interests

The authors declare no competing financial interests.

Methods

Atomically ordered Pb(110) surfaces were prepared from a bulk single crystal by several cycles of argon ion sputtering followed by annealing at 250 °C. To produce the Fe chains, electron beam evaporation of Fe was performed with the substrate held at approximately 85 °C, followed by 7 min of annealing at 175 °C. The sample was then gradually cooled for approximately 30 min and inserted into the STM. Ultrahigh vacuum conditions were maintained throughout this process.

To grow Pb overlayers on the Fe chain samples described above, we used a commercial Knudsen cell and a customized cooling stage to control the sample temperature during evaporation. The Pb evaporator was thoroughly degassed and was calibrated by means of a quartz crystal monitor. The temperature of the cooling stage was stabilized by the liquid nitrogen flow rate and the heater installed in the cooling stage. For the data shown in Fig. 5, we first grew Fe chains on a clean Pb substrate and then cooled the sample to 80 K. The buried Fe chain was prepared by evaporating 5 Å of Pb at an evaporation rate of 0.3 Å min^{-1} on the cold sample, followed by annealing at 158 K for 10 min on the same cooling stage.

Except where noted, dilution refrigerator experiments were performed using a setpoint bias of $V_{set} = -5$ mV, a setpoint current $I_{set} = 500$ pA, and an a.c. r.m.s. excitation of 20 μV. When combined with the 250 mK temperature, this leads to an expected experimental broadening of approximately 90 μeV. Assuming Gaussian peaks with a 90 μeV full-width at half-maximum, we expect to resolve two split peaks when they are separated by at least 80 μeV. Superconducting Pb tips were prepared by indentation of W tips into the Pb substrate.

Data availability. The data that support the plots within this paper and other findings of this study are available from the corresponding author upon reasonable request.